

Rashba and intrinsic spin-orbit interactions in biased bilayer graphene

Ralph van Gelderen* and C. Morais Smith

Institute for Theoretical Physics, Utrecht University, Leuvenlaan 4, 3584 CE Utrecht, The Netherlands
 (Received 9 November 2009; revised manuscript received 18 February 2010; published 26 March 2010)

We investigate the effect that the intrinsic spin-orbit and the interlayer and intralayer Rashba interactions have on the energy spectrum of either an unbiased or a biased graphene bilayer. We find that under certain conditions, a Dirac cone is formed out of a parabolic band and that it is possible to create a “Mexican hat”-like energy dispersion in an unbiased bilayer. In addition, in the presence of only an intralayer Rashba interaction, the K (K') point splits into four distinct ones, contrarily to the case in single-layer graphene, where the splitting also takes place, but the low-energy dispersion at these points remains identical.

DOI: 10.1103/PhysRevB.81.125435

PACS number(s): 73.20.At, 71.70.Ej, 73.21.Ac

I. INTRODUCTION

The influence of spin-orbit (SO) interactions on a single layer of graphene is well known. Kane and Mele^{1,2} were the first who showed that the intrinsic SO (ISO) interaction not only can open a gap, but it also gives rise to a quantum spin Hall phase, due to localized edge states. On the other hand, the extrinsic Rashba SO interaction acts in the opposite direction and tends to close the gap. Later, it was found that the Rashba interaction has interesting effects on its own, leading to a splitting of the Dirac point into four identical points.³ This splitting is missed in the low-energy calculations used in Refs. 1 and 2.

The presence of a gap controlled by the ISO interaction seemed promising but it turned out to be smaller than originally expected by Kane and Mele.^{4,5} The value of its coupling constant is still controversial, but is expected to be in the range 0.0011–0.05 meV,^{6,7} thus very small. The Rashba coupling instead, can be tuned to much higher values. For typical values of an external electric field (50 V/300 nm), the Rashba coupling is less than 1 meV.^{8,9} The effect of impurities can increase this value to 7 meV.¹⁰ However, recent experiments on epitaxial graphene grown on a Ni(111) substrate showed that the Rashba coupling can reach values up to 0.2 eV.¹¹

Shortly after the discovery of graphene, it was observed that bilayer graphene also exhibits remarkable phenomena. In bilayers, the low-energy excitations are no longer Dirac fermions, like in graphene, but massive chiral fermions due to the parabolicity of the energy bands.¹² In addition, bilayer graphene turns out to be a semiconductor with a gap that can be tuned via a chemical doping¹³ or by an external gate voltage.^{14–19}

Although there are several studies for the effect of SO interactions in graphene accounting for different boundaries^{3,20} (zigzag and armchair) and electron-electron interactions,⁵ no investigations of the SO effects have so far been performed in bilayer graphene, to the best of our knowledge. In this paper, we incorporate SO interactions in a bilayer graphene system in the presence and absence of a bias voltage. We distinguish between the ISO interaction, which respects the inversion symmetry of the graphene lattice and the extrinsic Rashba interaction, which is only present if this symmetry is broken. Here, we break the lattice

symmetry by introducing an electric field. Depending on the orientation of this electric field, there can be both intralayer as well as interlayer Rashba interactions. Furthermore, we consider how the energy spectrum deforms if the layer is biased with an electrical voltage.

As a main result, we find that the intralayer Rashba coupling in an unbiased bilayer not only splits the K (K') points into four, in a different way than it does for monolayer graphene,³ but also creates a Dirac cone out of a parabolic band. In addition, we show that a fully spin-polarized Mexican-hat band arises in the energy spectrum of an unbiased layer, purely due to SO interactions.

The Mexican-hatlike dispersion appears in a variety of physical systems. This kind of spectrum, with a line of degenerate low-energy points forming a ring, was first discussed by Brazovskii,²¹ who showed that it leads to a “weak” crystallization transition. In cold atoms physics, a Mexican-hatlike dispersion appears and gives rise to topologically different ground states in SO Bose-Einstein condensates.²² The Mexican hat is known in high-energy physics as well, where, for example, the Higgs mechanism is expected to be responsible for the mass of the vector bosons. For bilayer graphene without SO interactions, the energy dispersion has the Mexican-hat shape if the layers are biased. In this case the dispersion was shown to potentialize electron-electron interactions, thus leading to a ferromagnetic instability.²³

The outline of this paper is the following: to render the comparison with a monolayer sample easier, we recall some results for monolayer graphene in Sec. II. Next, we set up a model for bilayer graphene in Sec. III, after which we include SO interactions within the layers in Sec. IV. In Sec. V, we also include Rashba interactions between the layers, and in Sec. VI we show that the results remain valid even if next-nearest-neighbor (nnn) hopping is included. Finally, we draw our conclusions in Sec. VII.

II. SO INTERACTIONS IN MONOLAYER GRAPHENE

In graphene, the carbon atoms arrange themselves in a honeycomb lattice. Because there are two inequivalent positions for the carbon atoms, this honeycomb lattice can be seen as a triangular lattice with two atoms per unit cell, called A and B, see Fig. 1. In the tight-binding approach, one assumes that the electrons are localized around the lattice

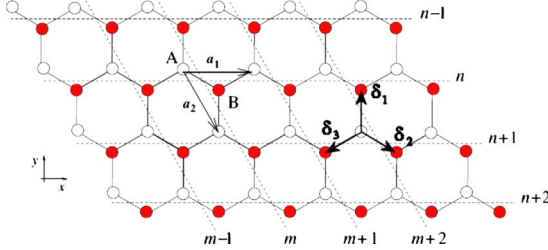


FIG. 1. (Color online) Relabeling of the graphene lattice. The length of the lattice vectors shown equals a while the lattice spacing is $a/\sqrt{3}$. Figure extracted and modified from Ref. 24.

sites and that they can hop from one lattice site to the next (nearest-neighbor hopping). The noninteracting Hamiltonian is then given by

$$H_0 = t \sum_{\substack{i \in \Lambda_A, \sigma \\ j=1,2,3}} [a_\sigma^\dagger(\mathbf{R}_i)b_\sigma(\mathbf{R}_i + \boldsymbol{\delta}_j) + H.c.], \quad (1)$$

where σ is the spin index, i runs over the A-sublattice sites, and j over the nearest-neighbor vectors, which, with a lattice orientation as in Fig. 1, are defined by

$$\begin{aligned} \boldsymbol{\delta}_1 &= \frac{a}{\sqrt{3}}(0,1), \\ \boldsymbol{\delta}_2 &= \frac{a}{\sqrt{3}}\left(\frac{\sqrt{3}}{2}, -\frac{1}{2}\right), \\ \boldsymbol{\delta}_3 &= \frac{a}{\sqrt{3}}\left(-\frac{\sqrt{3}}{2}, -\frac{1}{2}\right). \end{aligned}$$

The constant t is the hopping parameter (≈ 3 eV) and $a/\sqrt{3} \approx 0.142$ nm is the lattice spacing.

After relabeling the lattice as in Fig. 1, one can bring Hamiltonian (1) into the form

$$\begin{aligned} H_0 = t \sum_{n,m,\sigma} & [a_\sigma^\dagger(m,n)b_\sigma(m,n) + a_\sigma^\dagger(m,n)b_\sigma(m-1,n) \\ & + a_\sigma^\dagger(m,n)b_\sigma(m-1) + H.c.]. \end{aligned}$$

By performing a Fourier decomposition, the free Hamiltonian reads

$$H_0 = t \int d^2k \psi^\dagger(k) M_{4 \times 4}^0 \psi(k), \quad (2)$$

where $\psi^\dagger(k) = [a^\dagger(k)_\uparrow, a^\dagger(k)_\downarrow, b^\dagger(k)_\uparrow, b^\dagger(k)_\downarrow]$,

$$M_{4 \times 4}^0 = \begin{pmatrix} 0 & 0 & \gamma_k & 0 \\ 0 & 0 & 0 & \gamma_k \\ \gamma_k^* & 0 & 0 & 0 \\ 0 & \gamma_k^* & 0 & 0 \end{pmatrix},$$

and $|\gamma_k|^2 = 3 + 2 \cos(ak_x) + 4 \cos(ak_x/2) \cos(\sqrt{3}/2ak_y)$. The eigenvalues of H_0 are the well-known energy bands of graphene,²⁴ $E_\pm = \pm t|\gamma_k|$. Both bands are degenerate with respect to the spin degrees of freedom.

If one wants to include SO interactions into the graphene system, one has to distinguish between the ISO interaction and the extrinsic Rashba term. The ISO interaction does respect all symmetries of the graphene lattice and has the form of a nnn hopping term,

$$H_{SO} = it_{SO} \sum_{\langle\langle i,j \rangle\rangle} \nu_{ij} c_i^\dagger s_z c_j.$$

In this expression, t_{SO} is the ISO coupling constant, s_z is the z-component Pauli matrix describing the spin, and c_j is either a_j or b_j , depending whether the index j labels an A- or B-sublattice site, respectively. The factor ν_{ij} is +1 if the nnn hopping is anticlockwise and -1 if it is clockwise (with respect to the positive z axis). Note that this term describes hopping within the same sublattice.

Using the relabeling of the lattice shown in Fig. 1 and performing a Fourier decomposition, the ISO Hamiltonian can be rewritten as

$$H_{SO} = \Delta_{SO} \int d^2k \psi^\dagger(k) M_{4 \times 4}^{SO} \psi(k), \quad (3)$$

where

$$M_{4 \times 4}^{SO} = \begin{pmatrix} \eta_k & 0 & 0 & 0 \\ 0 & -\eta_k & 0 & 0 \\ 0 & 0 & -\eta_k & 0 \\ 0 & 0 & 0 & \eta_k \end{pmatrix},$$

$$\eta_k = [1/(3\sqrt{3})][2 \sin(ak_x) - 4 \sin(ak_x/2) \cos(\sqrt{3}ak_y/2)] \quad \text{and} \\ \Delta_{SO} = 3\sqrt{3}t_{SO}.$$

The extrinsic SO interaction is the Rashba term, which is only present if the inversion symmetry of the graphene lattice, $z \rightarrow -z$, is broken. This can happen if the graphene sheet couples to a substrate or if an electric field is present. For a perpendicular electric field, $\mathbf{E} = E\hat{\mathbf{z}}$, the Rashba coupling has the form of a nearest-neighbor hopping term and is given by^{2,3,25}

$$H_R = it_R \sum_{\langle i,j \rangle} c_i^\dagger (\mathbf{s} \times \hat{\mathbf{d}}_{ij}) \cdot \hat{\mathbf{z}} c_j + H.c., \quad (4)$$

where the Rashba coupling t_R can be tuned by changing the electric field strength, \mathbf{s} is the vector of Pauli matrices, and $\hat{\mathbf{d}}_{ij}$ is the unit vector that connects the i and j lattice sites. This term describes nearest-neighbor hopping but it only couples nearest neighbors with opposite spin. This is clearly seen if we rewrite this term in the same way that we rewrote the other terms,

$$H_R = t_R \int d^2k \psi^\dagger(k) M_{4 \times 4}^R \psi(k), \quad (5)$$

where we have defined

$$M_{4 \times 4}^R = \begin{pmatrix} 0 & N_{2 \times 2} \\ N_{2 \times 2}^\dagger & 0 \end{pmatrix},$$

$$N_{2 \times 2} = \begin{pmatrix} 0 & i[\xi_1(k) + \xi_2(k)] \\ i[\xi_1(k) - \xi_2(k)] & 0 \end{pmatrix},$$

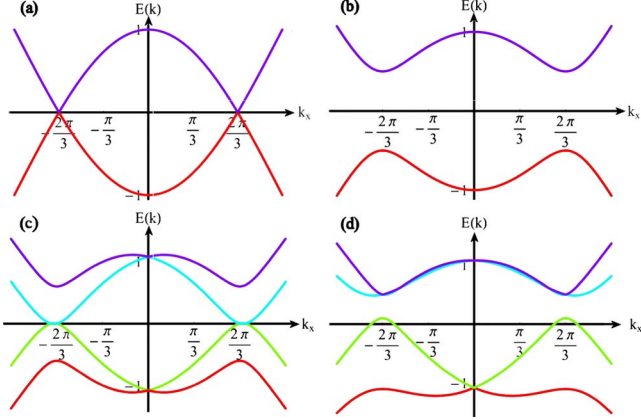


FIG. 2. (Color online) Behavior of a graphene sheet for different values of the SO parameters. (a) $\Delta_{SO}=0$ and $t_R=0$. (b) $\Delta_{SO}=0.5$ and $t_R=0$. (c) $\Delta_{SO}=0$ and $t_R=0.2$. (d) $\Delta_{SO}=0.5$ and $t_R=0.2$. Parameter values are $t=1$, $a=1$, and $k_y=2\pi/(\sqrt{3}a)$.

$$\xi_1(k) = e^{i(1/2)ak_x} \left[e^{-i(\sqrt{3}/2)ak_y} - \cos\left(\frac{1}{2}ak_x\right) \right],$$

$$\xi_2(k) = \sqrt{3}e^{i(1/2)ak_x} \sin\left(\frac{1}{2}ak_x\right).$$

The total Hamiltonian can be obtained by collecting Eqs. (1), (3), and (5),

$$H = \int d^2k \psi^\dagger(k) (tM_{4 \times 4}^0 + \Delta_{SO}M_{4 \times 4}^{SO} + t_R M_{4 \times 4}^R) \psi(k).$$

In Fig. 2 we show the behavior of the energy dispersion for a graphene sheet for different values of the SO parameters, Δ_{SO} and t_R , in units of t . Without SO interactions, we find the well-known graphene spectrum with Dirac cones centered at the K and K' points in the reciprocal space,²⁴ see Fig. 2(a). The ISO interaction opens a gap but respects the spin degeneracy of the energy bands [Fig. 2(b)]. The Rashba term does not open a gap on its own, but it does lift the spin degeneracy, except at the $k_x=0$ point, as it can be seen in Fig. 2(c). By zooming in on the region around the K (K') point, we see that the Rashba term splits the Dirac cones into four, as noted in Ref. 3. This behavior is depicted in Fig. 3. Note that this effect is missed in the approximation made by Kane and Mele,² which is effectively a zeroth-order approximation

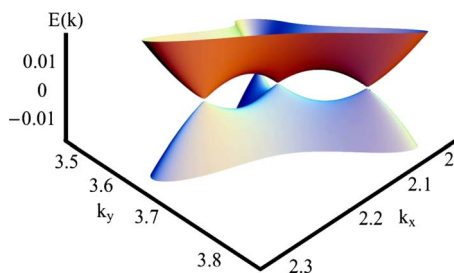


FIG. 3. (Color online) Splitting of the Dirac cones due to the Rashba interaction. For $\Delta_{SO}=0$ no gap opens. In this figure: $t=1$, $t_\perp=0.2$, $a=1$, $\Delta_{SO}=0$, and $t_R=0.2$.

of the Rashba term. If one takes linear terms in k into account, this effect is already present. Here, however, we keep the full expression for the spectrum, without resorting to approximations. The combined effect of the ISO interaction and the Rashba term breaks the particle-hole symmetry [Fig. 2(d)]. If the Rashba term is small ($t_R < \Delta_{SO}$), the gap is finite,² otherwise the gap closes (not shown).

III. BILAYER GRAPHENE MODEL

Before including the SO interactions into bilayer graphene, let us first consider the noninteracting Hamiltonian. The form of the Hamiltonian of a multilayer graphene system depends on the stacking of the layers.²⁴ For bilayers, however, there are only two possibilities. The lattice sites can lay exactly on top of each other, or they can be arranged in a Bernal stacking,²⁶ in which the A sites of the upper layer (A_1) lay on top of the B sites of the lower one (B_2), while the other sites (B_1 and A_2) lie opposite to a honeycomb center. We will assume the Bernal stacking here because it is the most common one.

The consequence of a Bernal stacking is that, in a first approximation, the only interlayer hopping is between A_1 and B_2 sites. It is straightforward to generalize the noninteracting monolayer Hamiltonian to a bilayer one. First, we define

$$\Psi(k)^\dagger = (a_{\uparrow,1}^\dagger, a_{\downarrow,1}^\dagger, b_{\uparrow,1}^\dagger, b_{\downarrow,1}^\dagger, a_{\uparrow,2}^\dagger, a_{\downarrow,2}^\dagger, b_{\uparrow,2}^\dagger, b_{\downarrow,2}^\dagger),$$

where the layers 1 and 2 are represented by the corresponding index. We introduce an interlayer hopping parameter, $t_\perp \approx (0.1-0.2)t$, and bias the bilayer system with a gate voltage V . This gate voltage can be tuned externally and is such that the lower layer has an electric potential $-V$ while the upper layer has V . With this new parameters, the noninteracting Hamiltonian is given by

$$H_0^{bl} = \int d^2k \Psi^\dagger(k) M_{8 \times 8}^0 \Psi(k),$$

$$M_{8 \times 8}^0 = \begin{pmatrix} V\mathbb{I}_{4 \times 4} + tM_{4 \times 4}^0 & A \\ A^\dagger & -V\mathbb{I}_{4 \times 4} + tM_{4 \times 4}^0 \end{pmatrix},$$

$$A = \begin{pmatrix} 0 & 0 & t_\perp & 0 \\ 0 & 0 & 0 & t_\perp \\ 0 & 0 & 0 & 0 \\ 0 & 0 & 0 & 0 \end{pmatrix}. \quad (6)$$

If we consider $V=0$ for the moment, we see in Fig. 4(a) that the spectrum is different from the one for monolayer graphene. The dispersion at the K (K') points, where the valence and the conduction bands touch, is no longer linear, but parabolic. This means that in a low-energy approximation the quasiparticles become massive ($m \approx 0.054m_e$).²⁷ However, these particles are chiral with respect to sublattice pseudospin and are therefore massive chiral fermions,¹² which are a new type of quasiparticles, characteristic for bilayer graphene.

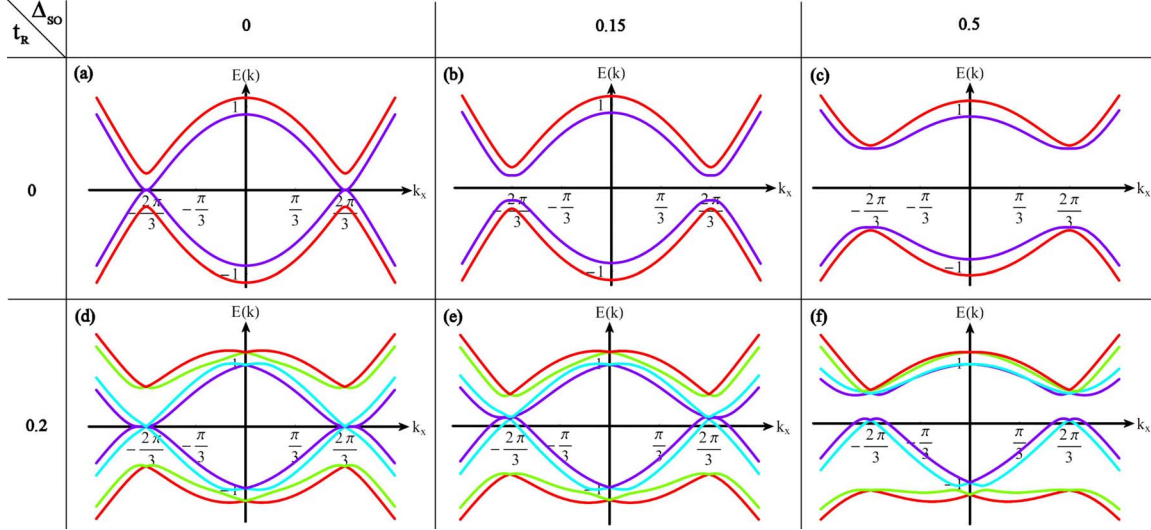


FIG. 4. (Color online) Energy spectrum of bilayer graphene for different values of the SO interactions. In this figure the layer is unbiased, hence $V=0$. Other parameters have the values $t=1$, $t_{\perp}=0.2$, $a=1$, and $k_y=2\pi/(\sqrt{3}a)$.

If there is a nonzero voltage difference, a gap will open in the energy spectrum. In fact, not only a gap opens, but the parabolic bands are deformed into Mexican hats in the vicinity of the K (K') points (see Ref. 18 and the discussion in Sec. IV B). However, the energy bands remain spin degenerate, because a nonzero voltage on its own cannot lift the spin degeneracy; as we will discuss in the next section, interactions are required to reach this aim.

IV. INTRALAYER SO INTERACTIONS IN BILAYER GRAPHENE

A. No bias voltage

Now that we have understood the single-particle spectrum for the bilayer graphene system, let us add SO interactions. We already saw that we have to distinguish between the ISO and the Rashba interactions, but for the bilayer system there is another subdivision, namely, into intralayer and interlayer interactions. In this section, we will analyze the effects that the intralayer ISO and Rashba couplings have on the energy spectrum of the bilayer system. The effect of these interactions in the presence of a bias voltage are subsequently discussed. Later we include also interlayer interactions. This is done in Sec. V.

The ISO interaction respects the symmetries of a single graphene sheet. Since a graphene bilayer has a smaller symmetry group than a single layer, we expect this interaction to be present in the planes of the bilayer system as well. The ISO interaction Hamiltonian is then given by

$$H_{SO} = \Delta_{SO} \int d^2k \Psi^\dagger(k) M_{8 \times 8}^{SO} \Psi(k), \quad (7)$$

$$M_{8 \times 8}^{SO} = \begin{pmatrix} M_{4 \times 4}^{SO} & 0 \\ 0 & M_{4 \times 4}^{SO} \end{pmatrix}. \quad (8)$$

Regarding the Rashba term, we expect that a perpendicular electric field gives rise to intralayer interactions in the

same way that it did for a single sheet of graphene. Effectively, we have two copies of the monolayer Rashba interaction,

$$H_R = t_R \int d^2k \Psi^\dagger(k) M_{8 \times 8}^R \Psi(k), \quad (9)$$

$$M_{8 \times 8}^R = \begin{pmatrix} M_{4 \times 4}^R & 0 \\ 0 & M_{4 \times 4}^R \end{pmatrix}. \quad (10)$$

In Fig. 4, the energy spectrum of an unbiased bilayer graphene is shown for different values of Δ_{SO} and t_R . For zero SO interactions, we observe the well-known parabolic bands, which are spin degenerate [see Fig. 4(a)]. These degeneracies cannot be lifted by the ISO interaction on its own, which simply opens a gap in the spectrum [Figs. 4(b) and 4(c)]. This is the same behavior as for monolayer graphene. Things become interesting when we consider the case of zero ISO coupling and a nonzero Rashba interaction [Fig. 4(d)]. The spin degeneracy of the bands is then lifted but in a very particular way. In Fig. 5(a), we see that for one of the spin bands [purple (or black) lines in Fig. 4(d)] the K point splits into four points again, as for monolayer graphene. One of them remains at the former K point position and the others form a triangle around it, see the inset in Fig. 5(a). We will refer to these four points as the split K point. However, here very special features appear: besides the two energy bands (conduction and valence band) that touch at four points, there are two more bands, associated with the other spin orientation [blue (or gray) lines in Fig. 4(d)], that touch and form a Dirac cone, as it can be seen in Fig. 5(b). The center of this Dirac cone is exactly at the point in k space where, without Rashba interaction, the K point was located. This is also the location of the central of the four points that form the split K point. This central point is different from the other three. If we analyze Fig. 6(a), which shows a zoom in of Fig. 4(d) and a cross-section cut of Figs. 5(a) and 5(b), we see that the central point, located at $k_x=2\pi/(3a)$, $k_y=2\pi/(\sqrt{3}a)$

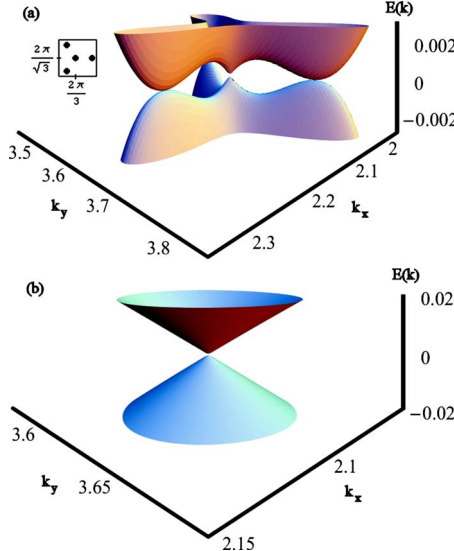


FIG. 5. (Color online) Due to the Rashba coupling, the spin degeneracy of the low-lying energy bands is lifted. (a) One band exhibits four touching points between the valence and the conduction bands. Inset: points in k space where the valence and the conduction bands touch. (b) The other band becomes a Dirac cone. In these figures, the layer is unbiased there is no ISO interaction, and $t_R=0.2$. Other parameters have the values $t=1$, $t_{\perp}=0.2$, and $a=1$.

has, in addition to the Dirac cone, a linear crossing at very low energy, whereas the off-center points have only a higher-order crossing. A zoom in on the satellites (not shown) seems to indicate that the crossing in the k_y direction is similar to that in the k_x direction. This is different from the case of monolayer graphene, where the K point splits into four equivalent points. The most striking feature of the intralayer Rashba coupling is the formation of a Dirac cone out of a parabolic band. If we perform a low-energy approximation and use $\mathbf{k}=\mathbf{K}+\mathbf{q}$, this Dirac cone has the dispersion relation $E(\mathbf{q})=\alpha|\mathbf{q}|$. The slope α , which corresponds to the velocity of the low-energy excitations, depends on the parameters of the theory and cannot be determined analytically. We have plotted the slope of this cone as a function of t_R for certain parameter values in Fig. 6(b).

If we set both t_R and Δ_{SO} unequal to zero [Figs. 4(e) and 4(f)], we see that depending on their relative values, a gap can open. For small ISO interactions, the gap stays closed, but the bands are heavily deformed in an asymmetric manner. Moreover, the particle-hole symmetry is lost. The split K point becomes so deformed that we cannot identify the four points any longer. If Δ_{SO} becomes large enough a gap opens but the asymmetry remains.

B. Effect of a bias voltage

If we add a bias voltage to a bilayer graphene system without SO interactions, the system becomes a semiconductor with a tunable gap. We will see in the following that SO interactions can heavily deform the energy dispersion.

As found earlier,^{16,24} we observe that for $\Delta_{SO}=t_R=0$ the effect of the bias is to open a gap and to introduce a Mexican-hatlike shape in the lowest energy band around the

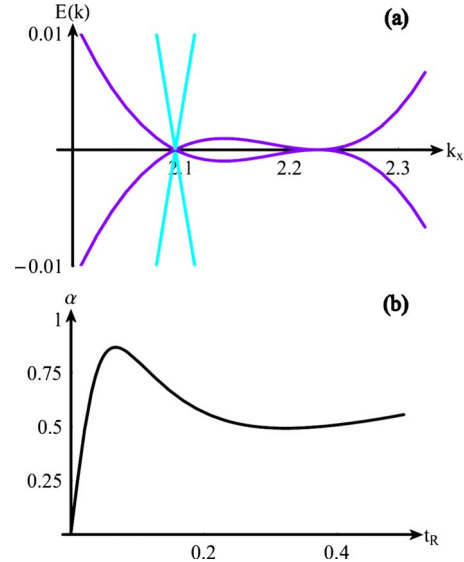


FIG. 6. (Color online) (a) Zoom in on the K point of Fig. 4(d) and an intersection along the line $k_y=2\pi/(\sqrt{3}a)$ of Fig. 5. (b) Slope (α) of the Dirac cone as a function of the Rashba coupling t_R . The scale of the α axis depends on all parameters of the theory. Here: $t=1$, $t_{\perp}=0.2$, $a=1$, $V=0$, $\Delta_{SO}=0$, and $k_y=2\pi/(\sqrt{3}a)$.

K and K' points. The spectrum remains particle-hole symmetric and the bands remain spin degenerate, as is shown in Fig. 7(a). By keeping $t_R=0$ and introducing a finite Δ_{SO} , the spin degeneracy is lifted, but only in the region around the K (K') points, as can be seen in Fig. 8(a). When Δ_{SO} is not too large, the Mexican-hat feature remains, but it disappears as Δ_{SO} is increased further [see Figs. 7(b) and 7(c)]. The gap at the K point (this is not the actual gap if $V>\Delta_{SO}$ because of the Mexican-hat structure), equals $2|V-\Delta_{SO}|$; Therefore, during the transition from the Mexican hat to a parabolic band the gap closes at $V=\Delta_{SO}$, after which it opens again. Note that this behavior is similar to that described in Ref. 1, where both the ISO coupling Δ_{SO} and a staggered sublattice potential λ_v can open a gap in monolayer graphene. If Δ_{SO} exceeds λ_v , a transition occurs between a normal insulator phase and a quantum spin-Hall phase. Nonetheless, we have to be careful with this comparison since a staggered sublattice potential in monolayer graphene is fundamentally different from a bias potential in a bilayer. For example, in monolayer graphene we do not observe a Mexican-hat structure and the edge states are responsible for the phase transition. We do not take those into account here. In addition, although the ISO interaction alone cannot lift the spin degeneracy, it does so in the presence of a staggered sublattice potential in monolayer graphene. The lifting occurs for all values of k , except for $k=0$, contrarily to the biased bilayer, where it is only significant around the K (K') points. Moreover, the effect is stronger in monolayer graphene than it is in bilayer graphene.

As long as the Rashba coupling is zero, an analytical solution for the energy bands can be found. This solution is given by

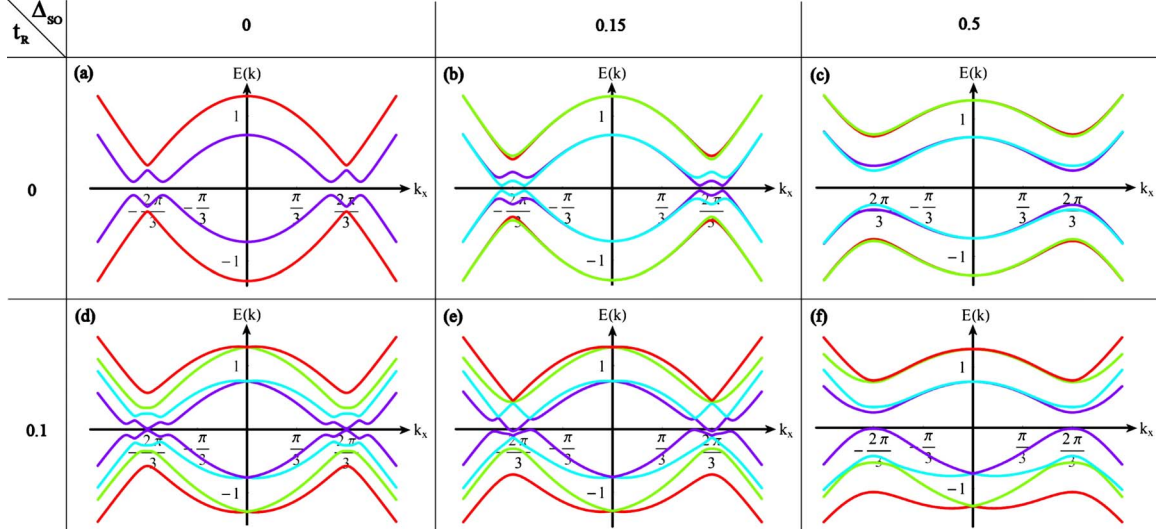


FIG. 7. (Color online) Energy spectrum of bilayer graphene for different values of the SO interactions. In this figure, the layer is biased, $V=0.25$. Other parameters have the values $t=1$, $t_{\perp}=0.2$, $a=1$, and $k_y=2\pi/(\sqrt{3}a)$.

$$\begin{aligned} E(k)^{\pm,\pm,\pm} = & \pm \frac{1}{\sqrt{2}} [t_{\perp}^2 + 2V^2 + 2t^2|\gamma|^2 \\ & + 2\Delta_{\text{SO}}^2\eta_k^2 \pm (t_{\perp}^4 + 4t^2t_{\perp}^2|\gamma|^2 + 16t^2V^2|\gamma|^2 \\ & + 16\Delta_{\text{SO}}^2V^2\eta_k^2 \pm 8t_{\perp}^2\Delta_{\text{SO}}V\eta_k]^{1/2}. \end{aligned} \quad (11)$$

In this expression, the three \pm correspond with conduction/valence band, upper/lower layer isospin (symmetric or antisymmetric combination of top and bottom layer states), and spin up/down, respectively. It is clear that, if either V , Δ_{SO} , or t_{\perp} is zero the bands become degenerate, since in this case the last term with the \pm sign vanishes. Another interesting feature that we see only in the particular situation, where t_{\perp} , V , $\Delta_{\text{SO}} \neq 0$, and $t_R=0$, is a band crossing at $k_x=0$ [see Figs. 7(b) and 7(c) and notice the inverted colors at the K and K' points], signaling that the $k_x \rightarrow -k_x$ symmetry is lost. This band crossing can be seen analytically from Eq. (11). Note that $|\gamma_k|^2$ is symmetric while η_k is antisymmetric under $k_x \rightarrow -k_x$. We conclude that, due to the linear term in η_k , the energy bands satisfies $E(k)^{\pm,\pm,\pm} = E(-k)^{\pm,\pm,\mp}$. Therefore, the individual bands are no longer symmetric under this transformation.

Now, let us investigate the behavior of the system at finite

t_R for $\Delta_{\text{SO}}=0$. First of all, the spin degeneracy is lifted except at $k_x=0$. Second, the Mexican-hat feature evolves into something that looks more like an asymmetric farmers hat, see Figs. 7(d) and 8(b). Note that if V and/or t_R are increased, the asymmetry becomes more accentuated and the spectrum does not even look like a farmers hat anymore. We must emphasize that here we do not use any approximation for the energy spectrum but we keep the full expression. This feature cannot be captured in a zeroth-order approximation for the Rashba term, as used by Kane and Mele,^{1,2} because at this order of the approximation the spectrum is symmetric around the K (K') point.

If both Δ_{SO} and t_R are finite, the spectrum becomes very complicated [Figs. 7(e) and 7(f)]. As a general trend, Δ_{SO} washes out the Mexican-hat feature and at first, increases the difference between spin-up and spin-down bands around the K (K') points, although the spin degeneracy had been already lifted for all values, except at $k_x=0$, by the finite Rashba coupling. In addition, particle-hole symmetry is lost. There is no longer a band crossing but the gap closes and opens again upon increasing Δ_{SO} . Depending on the parameters, a situation can occur where the bands do not touch, but they have common energies, thus there is no gap in the system [see Fig. 8(c)].

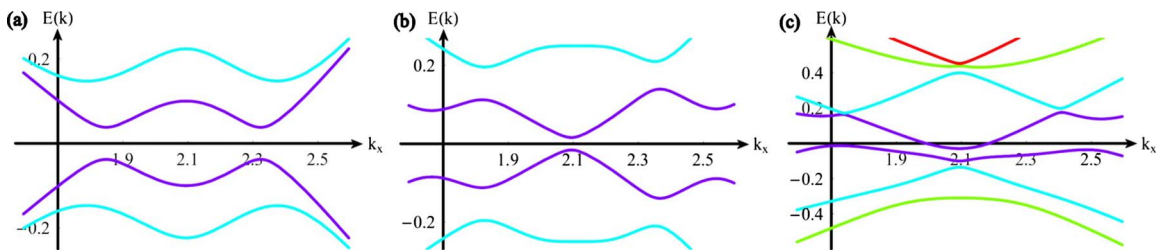


FIG. 8. (Color online) (a) Zoom in on the K point of Fig. 7(b). (b) Zoom in on the K point of Fig. 7(d). (c) Zoom in on the K point of Fig. 7(e). Recall that $V=0.25$, $t=1$, $t_{\perp}=0.2$, $a=1$, and $k_y=2\pi/(\sqrt{3}a)$.

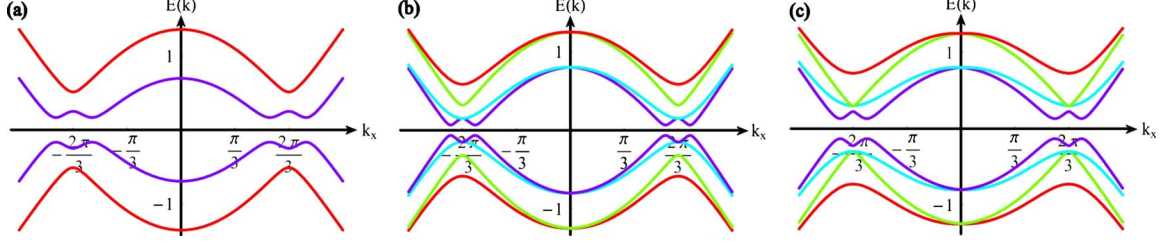


FIG. 9. (Color online) (a) Energy spectrum of a biased system, $V=0.25$, with zero intralayer SO interactions and $t_R^\perp=0.4$. Compare with Fig. 7(a). (b) Energy spectrum of an unbiased bilayer system, with zero intralayer Rashba coupling, but with $\Delta_{SO}=0.15$ and $t_R^\perp=0.4$. Compare with Fig. 4(b). (c) Energy spectrum of an unbiased bilayer system, with zero intralayer Rashba coupling, but with $\Delta_{SO}=0.3$ and $t_R^\perp=0.4$. Other parameters are $t=1$, $t_\perp=0.2$, $a=1$, and $k_y=2\pi/(\sqrt{3}a)$.

V. INTRALAYER AND INTERLAYER SO INTERACTIONS IN BILAYER GRAPHENE

In the previous section we accounted for tunneling between the two layers but considered only intralayer SO interactions. Now, we investigate the effect of SO interactions between lattice sites in different layers. Since the ISO interaction depends on the symmetry of the graphene plane, it is not obvious if there is any interplane ISO interaction at all. Hence, we focus on the Rashba term. This term only exists in graphene monolayers if the $z \rightarrow -z$ mirror symmetry is broken, for example, by a perpendicular electric field. Furthermore, the Rashba coefficient can be tuned by varying this electric field. Therefore, we consider here a bilayer system in the presence of a tilted electric field. The in-plane component of the electric field ($\mathbf{E}_{||}$) gives rise to an interlayer Rashba coupling that is a generalization of Eq. (4),

$$H_R^\perp = -it_R^\perp \sum_i a_{i,1}^\dagger (\mathbf{s} \times \hat{\mathbf{z}}) \cdot \hat{\mathbf{E}}_{||} b_{i,2} + \text{H.c.},$$

$$\hat{\mathbf{E}}_{||} = (\cos \phi, \sin \phi, 0)^T, \quad (12)$$

where we have chosen to absorb the magnitude of the electric field already in the constant t_R^\perp . The orientation of $\mathbf{E}_{||}$ is determined by ϕ but the results will be independent of ϕ and therefore we choose $\phi=0$ arbitrarily. The unit vector connecting the two lattice sites $A_{i,1}$ and $B_{i,2}$ is given by $-\hat{\mathbf{z}}$ and this explains the minus sign in comparison with Eq. (4). In k space, Eq. (12) becomes

$$H_R^\perp = t_R^\perp \int d^2k \Psi^\dagger(k) M_{8 \times 8}^{R,\perp} \Psi(k),$$

where the matrix $M_{8 \times 8}^{R,\perp}$ is given by

$$M_{8 \times 8}^{R,\perp} = \begin{pmatrix} 0 & C \\ C^\dagger & 0 \end{pmatrix}$$

with

$$C = \begin{pmatrix} 0 & 0 & 0 & -e^{-i\phi} \\ 0 & 0 & e^{i\phi} & 0 \\ 0 & 0 & 0 & 0 \\ 0 & 0 & 0 & 0 \end{pmatrix}.$$

The effect of this interlayer Rashba interaction depends heavily on the other parameters in the theory. Without any intralayer SO interactions, the result of a nonzero t_R^\perp is effectively a modification of the interlayer hopping parameter,

$$t_\perp \rightarrow t_\perp \sqrt{1 + (t_R^\perp)^2/t_\perp^2}. \quad (13)$$

The effect is a slight deformation of the energy bands. Only if $t_R^\perp \gtrsim 0.3$, the shift becomes significant. For a biased system, t_R^\perp will flatten the Mexican hat, as it can be seen in Fig. 9(a).

The effect of interlayer Rashba coupling is most visible in bilayer systems with zero bias but with intralayer ISO interactions. Although the energy spectrum can be solved analytically, the equations become too complicated to handle. However, it is clear that the effect is more than a shift of the interlayer hopping parameter. The spin degeneracy of the energy bands is lifted and we see a Mexican-hat feature appear in the low-lying energy band [see Fig. 9(b)]. These low-energy bands are shifted towards the Fermi level and as a consequence the gap between the valence and the conduction bands becomes smaller. If Δ_{SO} is small, the spin degeneracy of the lowest energy band stays intact at the K point, but is lifted around it. However, if Δ_{SO} increases, this degeneracy is lifted and eventually shifted to a degeneracy between the two conduction bands that lay in the middle, as it can be seen in Fig. 9(c). In comparison with the bilayer without intralayer interactions, the effect of nonzero t_R^\perp manifests itself also for small values of this parameter. In a biased system with intralayer ISO interactions, the effect of the interlayer Rashba coupling is visible, but its influence becomes less important as the bias becomes larger. The effect of a nonzero t_R^\perp in this case is to increase the splitting of the bands around the K (K') points and if $V > \Delta_{SO}$, the Mexican hat is flattened (not shown).

Let us now consider an unbiased system with zero ISO coupling but with nonzero interlayer and intralayer Rashba coupling. We would have such a system if a tilted electric field is present. The relative strength of both interactions can be tuned independently by changing the parallel and perpen-

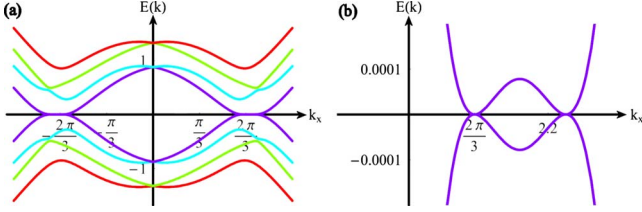


FIG. 10. (Color online) (a) Energy spectrum of an unbiased system with zero intralayer ISO interaction but $t_R=0.2$ and $t_R^\perp=0.4$. Compare with Fig. 4(d). (b) Zoom in on the K point of (a). Compare with Fig. 6(a). Other parameters are $t=1$, $t_\perp=0.2$, $a=1$, and $k_y=2\pi/(\sqrt{3}a)$.

dicular components of the electric field. This case is a generalization of the situation that lead to Fig. 4(d), which was described in more detail in Figs. 5 and 6. The most striking effect of a nonzero t_R^\perp is the lifting of the spin degeneracies at the K (K') points with as main consequence the destruction of the Dirac cones (see Fig. 10). The way the lowest-lying energy-band splits is also affected by the interlayer Rashba coupling. Recall that the K (K') point splits into four due to intralayer Rashba coupling and that the central point had a linear crossing at very low energy scales. This linear crossing is modified to a higher-order crossing by the interlayer Rashba interaction, as it can be seen in Fig. 10. Note that the energy scale of the zoom in at the K point in Fig. 10 has decreased by a factor 50 with respect to Fig. 6. This is also due to the interlayer Rashba coupling.

If all parameters are nonzero the spectrum is very complicated. Interlayer Rashba coupling does deform this spectrum but we could not detect any special feature that would justify exhibiting them.

VI. EFFECT OF OTHER HOPPING PARAMETERS

Until now we have completely neglected nnn hopping parameters. However, the values of the t_3 and t_4 parameters in the Slonczewski-Weiss-McClure (SWMc) model^{28,29} are comparable in magnitude with the values that we use for the SO interactions. In the SWMc model, t_3 is the amplitude for B_1-A_2 interlayer hopping, while t_4 describes either A_1-A_2 or B_1-B_2 hopping. There is a disagreement between the theoretical predictions and the experimental verifications of these parameters. Theoretically, t_3 is predicted to have a value of $t_3=0.3$ eV≈0.1 t ,²⁹ while from experiments one obtains that this parameter is a factor of three smaller,

$t_3=0.1$ eV≈0.033 t .³⁰ There is more agreement about the value of t_4 , namely, $t_4\approx 0.12-0.15$ eV≈0.05 t .²⁹ In monolayer graphene experiments, the Rashba coupling can be tuned already up to 0.2 eV≈0.068 t (Ref. 11) and this is comparable with the magnitude of the parameters we neglected. In this section we consider the SWMc model, which includes the nnn hopping parameters t_3 and t_4 , and verify whether the main results of the previous sections remain valid. Notice that in the previous sections we took the hopping parameter $t=1$ eV, whereas its real value is $t=3$ eV. Here we will use parameter values as realistic as possible and consider the most general model with higher-order hopping terms. Since the effects due to Δ_{SO} would only be visible for values of this parameter much larger than experimentally realizable, and these effects are not altered by the higher-order hopping terms, we will not include the intrinsic SO interaction here. In fact, Figs. 4 and 7–9 remain almost unaltered in framework of the full SWMc model.

The effect of t_3 on an unbiased bilayer without SO interactions is to introduce a splitting of the Dirac cone into four, the so-called trigonal distortion.²⁹ Indeed this effect, shown as the green/gray line in Fig. 11(a), is similar to the one produced by the intralayer Rashba interaction [blue/dashed line in Fig. 11(a)]. However, the splitting due to t_3 is smaller and the satellite points have a linear dispersion instead of the higher-order crossing we found in the bilayer with Rashba coupling. Remarkably, the two effects reinforce each other, as it is shown by the red/black line in the same figure. For certain values of the parameters t_R and t_3 , a situation can occur in which we can observe, instead of one satellite point as in the red curve of Fig. 11, two satellite points in the $k_y=2\pi/(\sqrt{3}a)$ direction (not shown). In fact, there are a total of seven touching points between the valence and the conduction bands in this case, namely, two satellite points in three different directions and the central point. The strength of the Rashba coupling that is needed to enter this regime depends heavily on the value of t_3 . For the theoretical value $t_3=0.3$ eV, the extra satellite points are visible on an energy scale of 0.01 meV, in the regime where $t_R\lesssim 0.4t_3$ or $t_R\gtrsim 3t_3$, while for the experimental value, $t_3=0.1$ eV, the extra satellite points can be seen (on the same energy scale), if $t_R\gtrsim 2t_3$. Since in the experimentally accessible cases the associated energies are very small, we do not go into further detail about the extra satellite points here. Another effect of the trigonal distortion is that the crossing of the bands at the satellite points becomes linear instead of higher order. However, the spin polarized Dirac cone remains intact. The for-

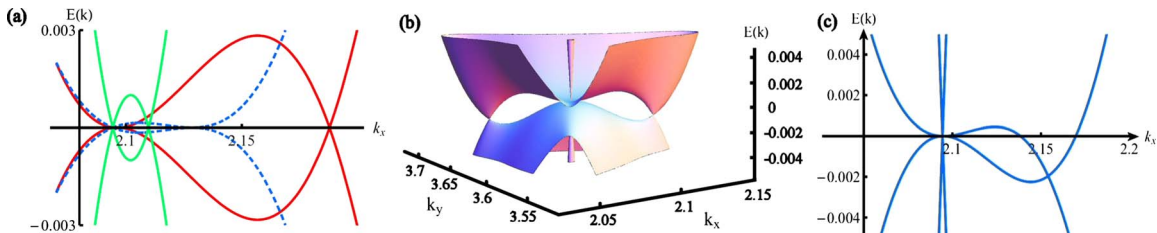


FIG. 11. (Color online) (a) Low-energy dispersion for $t_3=0.3$ eV, $t_R=0$ (green/gray line); $t_3=0$ eV, $t_R=0.3$ (blue/dashed line); and $t_3=0.3$ eV, $t_R=0.3$ (red/black line). Dirac cones are omitted. (b) Low-energy dispersion for parameter values $t_3=0.3$ eV, $t_4=0.1$ eV, and $t_R=0.2$ eV. (c) Cross-section cut of (b) along the line $k_y=2\pi/(\sqrt{3}a)$. Other parameter values are $t=3$ eV, $t_\perp=0.4$ eV, and $a=1$.

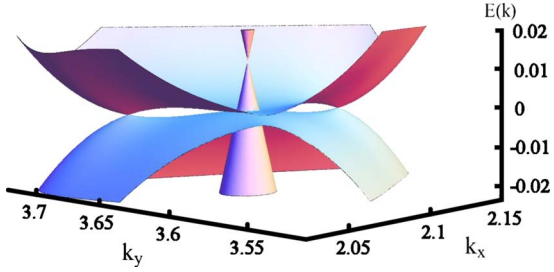


FIG. 12. (Color online) Plot for all parameters of the SWMc model nonzero. $t=3$ eV, $t_{\perp}=0.4$ eV, $a=1$, $t_3=0.3$ eV, $t_4=0.1$ eV, $\delta=0.018$ eV, and $t_R=0.2$ eV.

mation of this Dirac cone due to an intralayer Rashba coupling is therefore not affected by nonzero values for t_3 .

If one also includes A_1 - A_2 and B_1 - B_2 hopping via the parameter t_4 , the particle-hole symmetry is broken. This has consequences for the satellite points. In fact, the band crossing at these points is shifted below the Fermi level. This means that the conduction and the valence bands will overlap as can be seen in Figs. 11(b) and 11(c). Although it is possible, for certain parameter values, that the bands do not touch at all outside the K (K') points, they will touch for realistic values of t_3 and t_4 , but no longer at the Fermi energy [Figs. 11(b) and 11(c)]. Again, the Dirac cone is still present and there is no visible difference with the cone in the simplest model (not shown). There are still two different, spin polarized, low-energy excitations, namely, massless and massive quasiparticles. The difference is that before, the Fermi surface consisted of four points, whereas now it consists of a central point and three satellite pockets. The transport behavior should then change from semiconducting to metallic, when accounting for the t_4 term.

The SWMc model includes also a parameter $\delta \approx 0.018$ eV,²⁹ which is related to the onsite energy difference between stacked and unstacked sites. The sites that lie opposite to each other (A_1 and B_2) have a higher energy than the sites which are placed opposite to a honeycomb center. To incorporate this effect, an extra term is added to the Hamiltonian, $H_{\delta}=\delta\Sigma_i(a_1^{\dagger}a_1+b_2^{\dagger}b_2)$. This term affects the Dirac cone. However, it does not destroy it, but merely shifts the cone above the Fermi energy, as can be seen in Fig. 12. The shape of the cone remains unaltered. In fact, Fig. 6(b), which shows the slope of the cone, is exactly the same in the full SWMc model as it was in the simplified model we used before (not shown).

A last natural term to include into the model is an intralayer nnn hopping. This term shifts the position of the K and K' points along the energy axis. By doping the system, it is possible to shift the Fermi energy by the same amount and the final system would be identical to the one considered before. Therefore, this term is usually omitted.

VII. CONCLUSIONS

We studied a graphene bilayer including both, the intrinsic and the Rashba SO interactions, and we found that these interactions can modify the energy dispersion in a nontrivial

way. First, we concentrated on the unbiased system and considered only intralayer interactions. We observed that the ISO interaction can open a gap in the system in the same way as it does for monolayer graphene.² On the other hand, if only an intralayer Rashba SO interaction is present, the energy bands are completely different than for monolayer graphene. The K (K') points still split into four but at very low energies the off-center points have now a higher-order crossing instead of the linear crossing present in monolayer graphene [Fig. 6(a)]. The most striking feature, however, is the formation of a Dirac cone out of an energy band that once was parabolic [Fig. 5(b)]. This Dirac cone is located exactly at the former K (K') point. The intralayer Rashba interaction not only lifts the spin degeneracy of the energy bands but also changes their individual behavior. If both the intralayer ISO and Rashba terms are nonzero, the Dirac cone is destroyed and the particle-hole symmetry is broken.

The presence of a Dirac cone in unbiased bilayer graphene is a very special feature. Together with the split K (K') point, the spectrum that we found will give rise to two different low-energy excitations, one of which is massless. The speed with which this massless excitation travels depends on the Rashba constant [see Fig. 6(b)], which can be tuned by the perpendicular electric field. We expect that the dispersion relation shown in Fig. 6(a) could be observed with angle resolved photoemission spectroscopy (ARPES) experiments, which have already successfully demonstrated the Dirac dispersion in graphite.³¹

In a biased system with nonzero ISO interactions, the spin degeneracy of the energy bands is lifted. The splitting occurs only around the K (K') points. We also observe a band crossing at the $k_x=0$ point [Figs. 7(c) and 7(d)]. A bias voltage, in combination with the intralayer Rashba coupling, destroys the Dirac cones and the spectrum becomes asymmetric around the K (K') points.

Next, we considered an interlayer Rashba interaction between the planes. This interlayer interaction would, in principle, be expected to be small compared to the intralayer one because of the larger interlayer atomic separation. However, this effect could still be important if pressure is applied to approach the two layers. In our model, the interlayer Rashba coupling finds its origin in the presence of a tilted electric field. In a bilayer system with no intralayer SO interactions, this interaction causes effectively a shift of the interlayer hopping parameter. However, in a system where the intralayer SO couplings are nonzero, we see a clear effect in the energy spectrum. In an unbiased system with nonzero Δ_{SO} , the spin degeneracy of the bands is lifted around the K (K') points and a Mexican-hat feature appears. The Mexican-hat feature is known to arise in the bilayer system in the presence of a bias voltage.¹⁸ Here, however, we found that it can also appear without a bias, but solely due to SO interactions. Moreover, the Mexican-hat band in the energy dispersion is fully spin polarized. If the Δ_{SO} parameter becomes large enough, the degeneracy of the two lowest-lying conduction bands at the K (K') points is shifted to the two middle bands. The system then becomes isospin degenerate. Indeed, in the presence of tunneling, a bilayer can be described as a two-level system, where the energy bands in each layer have combined into symmetric and antisymmetric energy bands,

separated by a gap given by the tunneling energy. If we represent the asymmetric band by an isospin up and the symmetric one by an isospin down, we see that the ISO interaction can lead to an isospin degeneracy at the K and K' points, although the spins remain fully polarized.

If the ISO interaction is absent, but the intralayer Rashba is nonzero, we have seen in Fig. 10 that the effect of the interlayer Rashba interaction is to destroy the Dirac cone at the K (K') point and to modify the way the K (K') point splits into four. We can no longer observe a linear crossing for the central point and the energy scales associated with this splitting are substantially smaller.

Finally, we have checked the validity of our results when other parameters of the SWMc model are included. The higher-order hopping terms only affect the low-energy part of the spectrum, hence, only the results for an unbiased bilayer with nonzero intralayer Rashba interactions are visibly altered. The higher-order hopping term t_3 induces a trigonal distortion, a behavior which is also produced by the intralayer Rashba interaction. When both terms are present, the effect is amplified and the satellite points will lie further away from the center. On the other hand, the nnn hopping term t_4 breaks the particle-hole symmetry and shifts the touching points of the bands below the Fermi level, see Figs. 11(b) and 11(c). In all cases, the spin-polarized Dirac cone stays intact. When including the parameter δ of the SWMc model, which accounts for the energy difference between sites that lie opposite to each other and sites that lie opposite to a honeycomb center, we find that the cone is shifted away from the Fermi energy. The energy spectrum including all the parameters of the SWMc model is shown in Fig. 12.

Now, we would like to discuss the possibility of observing experimentally the effects that we have described above. In monolayer graphene, the current estimates are that the ISO interaction is very small (0.0011–0.05 meV).⁶ However, it is already possible to tune the Rashba coupling in a graphene layer on a Ni substrate up to $t_R \sim 0.2$ eV.¹¹ Because these values should be representative for bilayer graphene as well,

we expect that the results we found involving the Rashba interaction are well within the experimental reach. We believe that it should be possible to detect the Dirac cone that arises from the intralayer Rashba term in an unbiased bilayer. If this Dirac cone can be detected and if it is destroyed by an in-plane electric field, we would have an indication that indeed an interlayer Rashba interaction is present in the system.

The values we used for Δ_{SO} are larger than indicated experimentally. However, we should recall that the same kind of system could be engineered using cold atoms in optical lattices, and in this case there is much less constraint on the parameters of the model. It is already possible to create a two-dimensional honeycomb optical lattice³² and if a bilayer system could be mimicked, it should be possible to measure the single-particle spectrum.³³ In any case, our aim here was mainly to draw a comparison of the different effects of the Rashba and ISO interactions to determine the trend introduced by each one.

A next step would be to include edge states in the model. If we regard the intralayer ISO interaction and the bias voltage in bilayer graphene as being comparable with the ISO interaction and a staggered sublattice potential in monolayer graphene, there is a possibility that the bilayer system would exhibit a phase transition, equivalent to the one described in Ref. 1. It is already known that there are two types of edge states in bilayer graphene³⁴ but SO interactions have not yet been taken into account. We hope that our results will motivate further theoretical studies and experiments in the field.

ACKNOWLEDGMENTS

We acknowledge financial support from the Netherlands Organization for Scientific Research (NWO). We are grateful to, N. Sandler, W. Beugeling, and A. Lazarides for fruitful discussions. In particular, we would like to thank A. H. Castro Neto and M. Goerbig for their comments on the first draft of this paper.

*r.vangelderden1@uu.nl

¹C. L. Kane and E. J. Mele, Phys. Rev. Lett. **95**, 146802 (2005).

²C. L. Kane and E. J. Mele, Phys. Rev. Lett. **95**, 226801 (2005).

³M. Zarea and N. Sandler, Phys. Rev. B **79**, 165442 (2009).

⁴Y. Yao, F. Ye, X.-L. Qi, S.-C. Zhang, and Z. Fang, Phys. Rev. B **75**, 041401(R) (2007).

⁵M. Zarea and N. Sandler, Phys. Rev. Lett. **99**, 256804 (2007).

⁶S. Trickey, *Lecture Notes on Electronic States and Excitations on Nanostructures* (PASI School, Zacatecas, Mexico, 2007).

⁷J. C. Boettger and S. B. Trickey, Phys. Rev. B **75**, 121402(R) (2007).

⁸D. Huertas-Hernando, F. Guinea, and A. Brataas, Phys. Rev. B **74**, 155426 (2006).

⁹H. Min, J. E. Hill, N. A. Sinitsyn, B. R. Sahu, L. Kleinman, and A. H. MacDonald, Phys. Rev. B **74**, 165310 (2006).

¹⁰A. H. Castro Neto and F. Guinea, Phys. Rev. Lett. **103**, 026804 (2009).

¹¹Y. S. Dedkov, M. Fonin, U. Rudiger, and C. Laubschat, Phys. Rev. Lett. **100**, 107602 (2008).

¹²K. S. Novoselov, E. McCann, S. V. Morozov, V. I. Fal'ko, M. I. Katsnelson, U. Zeitler, D. Jiang, F. Schedin, and A. K. Geim, Nat. Phys. **2**, 177 (2006).

¹³T. Ohta, A. Bostwick, T. Seyller, K. Horn, and E. Rotenberg, Science **313**, 951 (2006).

¹⁴J. B. Oostinga, H. B. Heersche, X. Liu, A. F. Morpurgo, and L. M. K. Vandersypen, Nature Mater. **7**, 151 (2007).

¹⁵E. McCann, Phys. Rev. B **74**, 161403(R) (2006).

¹⁶E. V. Castro, K. S. Novoselov, S. V. Morozov, N. M. R. Peres, J. M. B. Lopes dos Santos, J. Nilsson, F. Guinea, A. K. Geim, and A. H. Castro Neto, Phys. Rev. Lett. **99**, 216802 (2007).

¹⁷E. Castro, K. Novoselov, S. Morozov, N. Peres, J. Lopes dos Santos, J. Nilsson, F. Guinea, A. Geim, and A. Castro Neto, arXiv:0807.3348 (unpublished).

¹⁸F. Guinea, A. H. Castro Neto, and N. M. R. Peres, Phys. Rev. B

- ⁷³, 245426 (2006).
- ¹⁹Y. Zhang, T.-T. Tang, C. Girit, Z. Hao, M. C. Martin, A. Zettl, M. F. Crommie, Y. R. Shen, and F. Wang, *Nature (London)* **459**, 820 (2009).
- ²⁰M. Zarea, C. B. Usser, and N. Sandler, *Phys. Rev. Lett.* **101**, 196804 (2008).
- ²¹S. A. Brazovskii, *Zh. Eksp. Teor. Fiz.* **68**, 175 (1975) [Sov. Phys. JETP **41**, 85 (1975)].
- ²²T. D. Stanescu, B. Anderson, and V. Galitski, *Phys. Rev. A* **78**, 023616 (2008).
- ²³T. Stauber, N. M. R. Peres, F. Guinea, and A. H. Castro Neto, *Phys. Rev. B* **75**, 115425 (2007).
- ²⁴A. H. Castro Neto, F. Guinea, N. M. R. Peres, K. S. Novoselov, and A. K. Geim, *Rev. Mod. Phys.* **81**, 109 (2009).
- ²⁵H. Engel, E. Rashba, and B. Halperin, Theory of Spin Hall Effects in Semiconductors, in *Handbook of Magnetism and Advanced Magnetic Materials*, edited by H. Kronmüller and S. Parkin, p. 2858, (John Wiley & Sons Ltd, Chichester, UK 2007).
- ²⁶Note that for bilayers there is no difference between Bernal stacking and rhombohedral stacking since they differ in the orientation of a possible third layer.
- ²⁷E. McCann and V. I. Fal'ko, *Phys. Rev. Lett.* **96**, 086805 (2006).
- ²⁸J. W. McClure, *Phys. Rev.* **108**, 612 (1957).
- ²⁹L. M. Zhang, Z. Q. Li, D. N. Basov, M. M. Fogler, Z. Hao, and M. C. Martin, *Phys. Rev. B* **78**, 235408 (2008).
- ³⁰L. M. Malard, J. Nilsson, D. C. Elias, J. C. Brant, F. Plentz, E. S. Alves, A. H. Castro Neto, and M. A. Pimenta, *Phys. Rev. B* **76**, 201401(R) (2007).
- ³¹S. Y. Zhou, G.-H. Gweon, J. Graf, A. V. Fedorov, C. D. Sparau, R. D. Diehl, Y. Kopelevich, D.-H. Lee, S. G. Louie, and A. Lanzara, *Nat. Phys.* **2**, 595 (2006).
- ³²G. Grynberg, B. Lounis, P. Verkerk, J.-Y. Courtois, and C. Salomon, *Phys. Rev. Lett.* **70**, 2249 (1993).
- ³³J. T. Stewart, J. P. Gaebler, and D. S. Jin, *Nature (London)* **454**, 744 (2008).
- ³⁴E. V. Castro, N. M. R. Peres, J. M. B. Lopes dos Santos, A. H. Castro Neto, and F. Guinea, *Phys. Rev. Lett.* **100**, 026802 (2008).